This is the accepted manuscript version of the final article:
Anna Rogowitz, Benjamin Huet, David Schneider, and Bernhard Grasemann (2015):
Influence of high strain rate deformation on 40Ar/39Ar mica ages from marble mylonites (Syros, Greece), Lithosphere, 7, 535-540
The final paper is accessible via http://dx.doi.org/10.1130/L455.1

The influence of high strain rate deformation on $^{40}Ar/^{39}Ar$ mica ages from marble mylonites (Syros, Greece)

Anna Rogowitz[1*], Benjamin Huet[1], David Schneider[2] and Bernhard Grasemann[1]
[1]Department of Geodynamics and Sedimentology
University of Vienna
Althanstrasse 14
Wien, A-1090
Austria
anna.rogowitz@univie.ac.at
Phone number (Department): +43-1-4277-53462

bernhard.grasemann@univie.ac.at
benjamin.huet@univie.ac.at

[2]Department of Earth Science
University of Ottawa
25 Templeton Avenue – ARC
Ottawa, Ontario K1N 6N5
Canada
david.schneider@uottawa.ca

ABSTRACT

Interpreting isotopic ages as deformation ages acquired from moderate temperature metamorphic environments can be a challenging task. Syros Island (Cyclades, Greece) is famous for Eocene high-pressure metamorphic rocks reworked by localized Miocene greenschist facies deformation. In this work we investigate phengites from coarse-grained marbles, which experienced the high-pressure event, and phengites from fine-grained localized marble shear zones attributed to the low-grade Miocene deformation. Based on structural criteria, both events can be easily discriminated because of their opposing kinematics. Laser-heating $^{40}Ar/^{39}Ar$ analysis on phengite yielded a 40 ± 1.6 Ma age for the host rock and a 37 ± 1.3 Ma age for the shear zone. Both ages are statistically indistinguishable, consistent with the regional Eocene event, and not the Miocene deformation event that is responsible for the formation of the shear zone. Thermodynamic modelling indicates that the observed high variance mineral assemblage is stable without compositional change along the pressure-temperature path followed by the rocks of Syros. Although the marble within the shear zone was deformed at extremely fast strain rates (10^{-10} s^{-1}), we observe no intracrystalline deformation of phengite grains and no resetting in the isotopic system because strain was mostly accommodated by calcite. Consequently, a high strain rate does not necessarily create deformation ages in rocks with high variance assemblages, such as marble mylonites.

KEYWORDS

strain partitioning, phengite, $^{40}Ar/^{39}Ar$ geochronology, deformation age, marble mylonite

INTRODUCTION

$^{40}Ar/^{39}Ar$ geochronology on white mica is a popular method to date deformation under greenschist facies temperature conditions (e.g. Dunlap, 1997; de Sigoyer et al., 2000; Bröcker et al., 2004; Rolland et al., 2009; Gébelin et al., 2011; Sanchez et al., 2011; Lanari et al., 2012; Schneider et al., 2013; Cossette et al., 2015). Most of the investigations applying such an approach have studied shear zones in a variety of quartzofeldspathic rock (e.g. quartzite, pelites, granites, gneisses) and concluded high strain events result in a distribution of apparent ages that scatter over 10-20 m.y.

In metasedimentary packages under upper greenschist to lower amphibolite metamorphic conditions, deformation tends to localize in calcite marbles resulting in the formation of mylonites and ultramylonites (Bestmann et al., 2000). In such rocks however, little is known about the behaviour of the K/Ar system in mica and the influence of high strain, particularly with reference to potential inefficient removal of ^{40}Ar from the grain boundary (Warren et al., 2012).

Several models invoke deformation-related Ar-loss and therefore may justify the interpretation of mica dates as deformation ages. For example, Goodwin and Renne (1991) proposed that due to deformation-related ductile or brittle grain size reduction, diffusion length scales are reduced and consequently volume diffusion becomes more efficient. Moreover, Ar loss during mica re- or neocrystallization, resets the K/Ar system potentially resulting in mixed ages (e.g. Wijbrans & McDougall, 1986; Foster & Lister, 2004; Cossette et al., 2015). From a crystallographic perspective, strong intracrystalline deformation is always accompanied by an increase in dislocation density in the crystals which may act as high diffusivity pathways, resulting in Ar loss by increased pipe-diffusion along dislocation lines (Lee, 1995; Dunlap & Kronenberg, 2001). Consequently, pipe diffusion has a lower activation energy and larger diffusion coefficient than volume diffusion and is therefore the dominant mechanism (Kramer et al., 2001; Dunlap & Kronenberg, 2001).

Because of possible physiochemical mechanisms leading to Ar loss during deformation, the interpretation of geochronological data requires detailed microstructural and geochemical analyses. Building off of our recent study in which we characterize microfabrics and corresponding deformation mechanisms at different strain rates (Rogowitz et al., 2014), we use the same outcrop on Syros (Cyclades, Greece) to assess the extent of K/Ar resetting due to extremely localized deformation in marbles. Our study presents ^{40}Ar/^{39}Ar ages from two marble samples that followed the same P-T-t path but witnessed contrasting strain intensities at different strain rates. We suggest that high strain rate in high variance assemblages does not necessarily reset the K/Ar system in phengite.

GEOLOGICAL SETTING AND OUTCROP DESCRIPTION

Syros Island is part of the Cycladic blueschist belt that is situated in the back-arc of the Hellenic subduction zone (Papanikolaou, 1987; Wortel et al., 1993). The Cycladic area is composed of three main units, separated by tectonic contacts, which are from bottom to top: the para-autochthonous Basement Unit, the Cycladic Blueschist Unit (CBU) and the Upper Unit (e.g. Bonneau, 1984; Jolivet & Brun, 2010).

Syros is dominated by the CBU, with an Upper Unit klippe exposed in the south-east (Tomaschek et al., 2000; Keiter et al. 2011; Soukis & Stockli, 2013). Two major Cenozoic metamorphic events have affected the Cyclades (Jolivet & Brun, 2010; Ring et al., 2010). An Eocene M1 eclogite-blueschist facies event which is associated with top-to-west sense of shear along the western margin of Syros and an Oligo-Miocene M2 greenschist facies event that is associated with dominant top-to-east sense of shear. Both events are well documented on Syros (Gautier & Brun, 1994; Trotet et al., 2001a; Bond et al., 2007; Keiter et al., 2011; Philippon et al., 2011). Geochronology performed on eclogite and blueschist facies rocks, including ^{40}Ar/^{39}Ar and Rb-Sr ages on white mica, U-Pb on zircons and Lu-Hf on garnet, yield ages between 52-37 Ma for M1 tectonism on Syros (Tomaschek et al., 2003; Lagos et al., 2007; Bröcker et al., 2013) whereas ^{40}Ar/^{39}Ar and Rb-Sr geochronology performed on greenschist facies rocks result in ages around 23-19 Ma for the greenschist facies overprint (Bröcker et al., 2013).

Our study focuses on an outcrop in the western part of Syros north of Delfini (UTM35 414840N 313839E). It exposes a decameter-scale thick calcite marble layer intercalated with quartz and dolomite lenses, preserving an E-W trending lineation and two different shear kinematic directions. Quartz and dolomite layers are deformed with asymmetric shearband boudinage indicating top-to-west shearing (Goscombe et al., 2004; Fig. 1A, B). The higher temperatures required for ductile deformation of dolomite and quartz together with the observed top-to-west sense of shear suggests that these structures are related to the Eocene M1 event. Conversely, flanking structures, calcite sigma clasts and localized shear zones in calcite marble show M2 related top-to-east shearing (Fig. 1C, D). We collected samples from a 5 m-long a-type flanking structure located in an almost pure calcite marble as part of a larger study (Rogowitz et al., 2014, Fig.1D). The flanking structure developed due to the rotation of a crack (i.e. cross-cutting element) during top-to-east shearing, resulting in antithetic slip along the cross-cutting element and the formation of a secondary shear zone with a maximum displacement of 120 cm (Grasemann & Stüwe, 2001; Passchier, 2001). As a consequence of overall top-to-east shearing, local antithetic top-to-west sense of shear is observed within the secondary shear zone (Rogowitz et al., 2014).

METHODS

Two samples, from the host rock (HR) and the shear zone (SZ) were collected for detailed microstructural, geochemical and $^{40}Ar/^{39}Ar$ analyses (Fig. 1D). Carbon coated, mechanically polished thin-sections were prepared for microstructural analysis. Modal composition and microstructures were analysed via optical microscopy (Leica DM4500 P) and scanning electron microscopy in back scattered electron mode (SEM-BSE, FEI Inspect S, FEI Quanta 3D FEG; University of Vienna, Austria) operated at an accelerating voltage in a range between 10 and 15 kV and a current of 4 nA. Quantitative electron microprobe (EMP) analyses was performed on a Cameca SX-100 (University of Vienna, Austria) at an accelerating voltage of 15 kV and a current of 20 nA with a defocused beam up to 7 µm in diameter. In order to evaluate the scattering of chemical analyses due to analytical uncertainties, we carried out a Monte Carlo simulation following the method of Lanari et al. (2014). For each sample, a population of 50 analyses was generated using the sample average analysis and analytical uncertainties calculated based on EMP counts. The structural formula was then calculated for each simulated analysis.

Incrementally step-heated $^{40}Ar/^{39}Ar$ geochronology on hand-picked phengite separates was performed with a Photon Machines CO_2 laser coupled to a Nu Instruments Noblesse multicollector mass spectrometer housed at the Geological Survey of Canada (Ottawa, Canada). Grain size ranges between 106 and 250 µm, and 3-4 grain aliquots were used for the analysis following the protocol of Kellett & Joyce (2014; the complete methodology and analytical details are described in the supplementary material). Our preferred ages are calculated as the weighted mean of a selection of mostly contiguous increments which represent >50% of ^{39}Ar gas released and result in concordant ages.

RESULTS

Flanking structures develop at relatively low strain (γ <5; Kocher & Mancktelow, 2005). Calculations by Rogowitz et al. (2014) show that the host rock on Syros experienced a shear strain of γ <3 during the formation of the flanking structure.

However, the rocks within the shear zone experienced a much higher shear deformation, having a maximum displacement of 120 cm at the centre of the shear zone where the width is only 1.5 cm. This corresponds to a shear strain of $\gamma \sim 80$. A differential stress-grain size deformation mechanism map for calcite at 300 °C was calculated showing that the host rock has been deformed at strain rates of $\sim 10^{-12}$ s^{-1} whereas within the shear zone, strain rates reached 10^{-10} s^{-1} (Rogowitz et al., 2014). Based on strain and strain rate data, the interval of deformation is estimated to have lasted ca. 25 kyr.

The marble is composed of nearly pure calcite with minor amounts of dolomite (<10%), quartz (<1%) and phengite (<1%). Microstructure of the host rock is characterized by coarse calcite grains with an average grain size of 280 µm. Minor undulatory extinction and slightly curved grain boundaries indicate that minor deformation took place within the calcite dislocation creep field (Fig. 2A). Within the shear zone, strong intracrystalline deformation, subgrain formation and subsequent recrystallisation lead to the formation of alternating protomylonitic and ultramylonitic calcite layers (Fig. 2B).

In both samples, phengite (long axis <400 µm) is preferentially orientated parallel to the foliation (Fig. 2C, D) defining the lineation together with the shape-preferred orientation of calcite. Phengite grains behave brittle rather than ductile, and experience minor grain size reduction by splitting and breaking preferentially along the cleavage resulting in prismatic or columnar shapes (Fig. 2C-F). In ultrafine grained (3 µm) layers within the shear zone fracturing perpendicular to the phengite cleavage plane can be observed (Fig. 2F).

Mineral chemistry analyses reveal that in both samples the phengite has a relatively high Si content (3.4-3.6; Fig. 3A). The Fe content is almost below the detection limit of around 500 ppm, resulting in an X_{Mg} greater than 0.97. The end-member composition of the phengite in both samples is around 50% muscovite, 45% celadonite and smaller amounts of paragonite and pyrophyllite (Fig. 3B). Chlorine and fluorine concentrations are below the detection limit. Except for the slight Fe content variance, there is no distinct difference in chemical composition of phengite located in the host rock and the shear zone. Mineral chemical analyses and SEM-BSE images indicate homogeneous phengite composition (Fig. 2E, F).

Ages obtained by step-heated $^{40}Ar/^{39}Ar$ geochronology from both the host rock and shear zone are statistically undistinguishable (Fig. 4A; Table S1 in the supplementary material), and total gas ages are concordant to preferred ages. The age spectrum for phengite located within the host rock exhibits a slightly disturbed age spectra with single step ages varying between 32 and 41 Ma yielding a preferred $^{40}Ar/^{39}Ar$ age of 40.2 ± 1.6 Ma. The age spectrum for phengite located within the shear zone is less disturbed, with little variation in single step ages between 36 and 40 Ma, yielding a preferred $^{40}Ar/^{39}Ar$ age of 37.4 ± 1.3 Ma. A $^{38}Ar/^{39}Ar$ versus $^{37}Ar/^{39}Ar$ diagram shows a clear data cluster for the shear zone phengite, indicating an isochemical Ar population whereas data for the host rock are variable, consistent with the more disturbed age spectra for host rock mica (Fig. 4B).

DISCUSSION

Observed marble microstructures from the outcrop on Syros are consistent with calcite deformation at ~300 °C (Bestmann et al., 2000, Rogowitz et al., 2014). Qualitative temperature estimates together with the top-to-east kinematics of the structure indicates that the flanking structure developed during the Miocene greenschist facies deformation. However, the $^{40}Ar/^{39}Ar$ mica ages for the host rock and shear zone of ca. 37-40 Ma correlate to the regional high pressure event (Bröcker et al., 2013), indicating that the phengite preserve the age of the older M1 event and not the formation of the Miocene flanking structure. Despite the expectation that the $^{40}Ar/^{39}Ar$ analyses from the calcitic mylonite should yield Miocene dates, apparently there was no resetting of the K/Ar system during deformation associated with shear zone formation. Although we have documented strain rates up to 10^{-10} s^{-1} (Rogowitz et al., 2014), we do not observe any phengite recrystallization and instead the calcite shows strong intracrystalline deformation by subgrain formation, undulatory extinction and recrystallization (Fig.2B). We therefore consider that the phengite was stronger than calcite during shearing, which fostered strain partitioning between the phases. This phenomenon has been documented elsewhere in the Cyclades on similar lithologies (Cossette et al., 2015) and is consistent with experiments on calcite-muscovite aggregates (Delle Piane et al., 2009) and evolution of two phase systems (Etchecopar, 1977; Handy, 1990) showing that once mica is rotated in the shear direction it behaves rather rigidly. The only deformation mechanism recorded in the phengite is therefore minor brittle deformation preferentially along the cleavage, which has been shown to be negligible for Ar loss at low temperatures (Dunlap & Kronenberg, 2001). Due to the short deformation interval (ca. 25 kyr) at low temperatures (~300 °C), which is below muscovite $^{40}Ar/^{39}Ar$ closure temperature (Hames & Bowring, 1994; Harrison et al., 2009), evidence for enhanced effective volume diffusion, due to reduced diffusion path lengths by brittle deformation perpendicular to the cleavage, can be excluded for our samples.

In addition to potassium, Ca and Cl concentrations are important factors when interpreting $^{40}Ar/^{39}Ar$ spectra since ^{37}Ar and ^{38}Ar can be derived from these elements, respectively (McDougall & Harrison, 1999), and may shed light on the homogeneity of a sample. The shear zone phengite is clearly isochemical, tightly clustering into a single population (Fig. 4B), indicating a single Ar reservoir. The host rock phengite is comparatively scattered, particularly with respect to ^{37}Ar. The somewhat heterogeneous $^{37}Ar/^{39}Ar$ versus $^{38}Ar/^{39}Ar$ distribution for host rock phengite may be explained by the presence of different Ar reservoirs (e.g. Foster & Lister, 2004) or is a result of minor Ca (as ^{37}Ar) contamination of calcite intergrown within or on the mica. Interestingly, although the $^{40}Ar/^{39}Ar$ analysis reveals two distinct chemical behaviours in Ar-isotope space, our mineral analyses illustrate that neither phengite sample exhibits chemical zoning and both samples are chemically homogeneous with respect to the major element chemistry. The observed scattering in Si content can be attributed to EMP uncertainties, as shown by a Monte Carlo analysis (Fig. 3A, Table S2 in the supplementary material).

The apparent homogeneous chemical composition of phengite for the host rock and shear zone can be explained by thermodynamic modelling (Fig. 5). An equilibrium phase diagram calculated for the rock composition suggests that the documented mineral assemblage (calcite/aragonite + quartz + dolomite + phengite) is stable over a wide range of fluid compositions and P-T conditions along the PT-path of Syros rocks (Trotet et al., 2001b; Schumacher et al., 2008). The parameters of the model include information on fluid composition, demonstrating that the mineral assemblage is also stable for CO_2 fractions between 0.005 and 0.03. Similar fluid compositions (XCO_2 <0.03) have been reported for impure marbles of Syros (Schumacher et al., 2008). Phengite being the only stable K- and Al-bearing phase over a wide range of

P-T conditions, a change in mica chemical composition by Tschermak and pyrophyllite substitution is not probable. The phengite chemistry is therefore stable within the marble's mineral assemblage and is not required to reequilibrate through prograde and retrograde conditions. If chlorite would have been present, the activation of these substitutions might have been possible resulting in potential resetting of K/Ar system.

Our study is certainly not an exhaustive one, and is meant to challenge the common approach of a field geologist sampling a shear zone in an attempt to resolve the age of deformation. In our investigation, we have surprising $^{40}Ar/^{39}Ar$ results from a field-based perspective. If, instead, we were able to conduct the same experiment in a set of quartzofeldspathic rocks, our results would be markedly different, and similar to other studies that report 10-20 m.y. scatter in apparent ages (e.g. Mulch et al., 2002; Cossette et al., 2015). Thus, we urge caution when dating micas from deformed calcite dominated assemblages.

CONCLUSION

1) Step-heated $^{40}Ar/^{39}Ar$ geochronology performed on phengite from host rock and shear zone marbles collected on Syros result in indistinguishable ages of ca. 40 Ma, reflecting the overall Eocene high-pressure event and not the Miocene deformation, which is recorded in structures with opposing kinematics.
2) Metamorphic conditions modelled from the preserved mineral assemblage do not require phengite re-equilibration during the Miocene event.

This is the accepted manuscript version of the final article:
Anna Rogowitz, Benjamin Huet, David Schneider, and Bernhard Grasemann (2015):
Influence of high strain rate deformation on 40Ar/39Ar mica ages from marble mylonites (Syros, Greece), Lithosphere, 7, 535-540
The final paper is accessible via http://dx.doi.org/10.1130/L455.1

3) Although marbles were deformed during the Miocene at extremely fast strain rates (10^{-10} s^{-1}) under greenschist facies conditions, calcite accommodated most of the strain, thus inhibiting phengite recrystallization.
4) Neither mechanical nor chemical processes caused any disturbance of the phengite crystal lattice and therefore the K/Ar system remained closed during the Miocene deformation event.
5) In accord with previous studies, it is emphasized that calcite marbles may not be the ideal host rock for resolving deformation ages. Moreover, it is the degree of mica recrystallization and not the amount of finite strain the rock has experienced in controlling the resetting of K/Ar systems at low temperatures.

ACKNOWLEDGMENTS

We thank the University of Vienna (grant number IK543002) for supporting the doctoral school DOGMA (“Deformation of Geological Materials”) and the Austrian Science Foundation FWF for funding the project “Mineral reactions and deformation in host-inclusion settings” (grant number I471-N19) as part of the international research group FOR741-DACH. Funding for DAS was provided by an NSERC Discovery grant. Detailed reviews by the reviewers Pierre Lanari and Yvette Kuiper, Klaus Gessner and efficient editorial handling by Arlo Weil are gratefully appreciated.

REFERENCES

Bestmann, M., Kunze, K., and Matthews, A., 2000, Evolution of a calcite marble shear zone complex on Thassos Island, Greece: microstructural and textural fabrics and their kinematic significance: Journal of Structural Geology 22, p. 1789-1807.

Bond, C.E., Butler, R.W.H., and Dixon, J.E., 2007, Co-axial horizontal stretching within extending orogens: the exhumation of HP rocks on Syros (Cyclades) revisited: The Geological Society, London, Special Publications 272, p. 203-222.

Bonneau, M., 1984, Correlation of the Hellenide nappes in the south-east Aegean and their tectonic reconstruction: The Geological Society, London, Special Publications 17, p. 517-527.

Bröcker, M., Bieling, D., Hacker, B., and Gans, P., 2004, High Si phengite records the time of greenschist-facies overprinting: implications for models suggesting mega-detachments in the Aegean Sea: Journal of Metamorphic Geology 22, p. 427-442.

Bröcker, M., Baldwin, S., and Arkudas, R., 2013, The geological significance of $^{40}Ar/^{39}Ar$ and Rb-Sr white mica ages from Syros and Sifnos, Greece: a record of continuous (re)crystallization during exhumation: Journal of Metamorphic Geology 31, p. 629-646.

Coggon, R and Holland, TJB, 2002. Mixing properties of phengitic micas and revised garnet-phengite thermobarometers, Journal of Metamorphic Petrology, 20, p. 683–696.

Connolly, J. A. D., 1990. Multivariable phase diagrams: an algorithm based on generalized thermodynamics. American Journal of Science 290, p. 666-718.

Cossette, É., Schneider, D.A., Warren, C., and Grasemann, B., 2015, Lithological, rheological and fluid infiltration control on $^{40}Ar/^{39}Ar$ ages in polydeformed rocks from the West Cycladic Detachment System, Greece: Lithosphere, doi:10.1130/L416.1.

Delle Piane, C., Wilson, C.J.L., and Burlini, L., 2009, Dilatant plasticity in high strain experiments on calcite-muscovite aggregates: Journal of Structural Geology 31, p. 1084-1099.

Dunlap, W.J., 1997, Neocrystallization or cooling? $^{40}Ar/^{39}Ar$ ages of white micas from low-grade mylonites: Chemical Geology 143, p. 181-203.

Dunlap, W.J., and Kronenberg, A.K., 2001, Argon loss during deformation of micas: constraints from laboratory deformation experiments: Contributions of Mineralogy and Petrology 141, p. 174-185.

Etchecopar, A., 1977, A plane kinematic model of progressive deformation in a polycrystalline aggregate: Tectonophysics, v. 39, p. 121–139.

Forster, M.A., and Lister, G.S., 2004, The interpretation of $^{40}Ar/^{39}Ar$ apparent age spectra produced by mixing: Application of the method of asymptotes and limits: Journal of Structural Geology 26(2), p. 287-305.

Gautier, P., and Brun, J.-P., 1994, Crustal-scale geometry and kinematics of late-orogenic extension in the central Aegean (Cyclades and Evia Island): Tectonophysics 238, p. 399-424.

Gébelin, A., Mulch, A., Teyssier, C., Heizler, M., Vennemann, T., Seaton, N., 2011. Oligo-Miocene extensional tectonics and fluid flow across the Northern Snake Range detachment system, Nevada. TECTONICS, VOL. 30, TC5010.

Goscombe, B.D., Passchier, C.W., and Hand, M., 2004, Boudinage classification:

end-member boudin types and modified boudin structures: Journal of Structural Geology 26, p. 739-763.

Goodwin, L.B., and Renne, P.R., 1991, Effects of progressive mylonitization on Ar retention in biotite from the Santa Rosa Mylonite Zone, California, and thermochronological implications: Contributions to Mineralogy and Petrology 108, p. 283-297.

Grasemann, B., and Stüwe, K., 2001, The development of flanking folds during simple shear and their use as kinematic indicators: Journal of Structural Geology 23, p. 715-724.

Hames, W.E., and Bowring, S.A., 1994, An empirical evaluation of the argon diffusion geometry in muscovite: Earth and Planetary Science Letters 108, p. 161-167.

Handy, M.R., 1990, The solid-state flow of polymineralic rocks: Journal of Geophysical Research, v. 95, p. 8647–8661, doi:10.1029/JB095iB06p08647

Harrison, T.M., Célérier, J., Aikman, A.B., Hermann, J., and Heizler, M.T., 2009, Diffusion of ^{40}Ar in muscovite: Geochimica et Cosmochimica Acta 73, p. 1039-1051.

Holland, T.J.B., Powell, R., 1998, An internally-consistent thermodynamic dataset for phases of petrological interest: Journal of Metamorphic Geology 16, p. 309-344.

Jolivet, L., and Brun, J.-P., 2010, Cenozoic geodynamic evolution of the Aegean: International Journal of Earth Sciences 99, p. 109-138.

Keiter, M., Piepjohn, K., Ballhaus, C., Lagos, M., and Bode, M., 2004, Structural development of high pressure metamorphic rocks on Syros island (Cyclades, Greece): Journal of Structural Geology 26, p. 1433-1445.

Keiter, M., Ballhaus, C., and Tomaschek, F., 2011, A new geological map of the Island of Syros (Aegean Sea, Greece): Implications for lithostratigraphy and structural history of the Cycladic Blueschist Unit: The Geological Society of America, Special Paper 481.

Kellett, D. and Joyce, N., 2014, Analytical details of single- and multicollection ^{40}Ar/^{39}Ar measurements for conventional step-heating and total fusion age calculation using the Nu Noblesse at the Geological Survey of Canada; Geological Survey of Canada, Technical Note 8, 27 p. doi: 10.4095/293465.

Kocher, T., and Mancktelow, N.S., 2005, Dynamic reverse modelling of flanking structures: a source of quantitative kinematic information: Journal of Structural Geology 27, p. 1346-1354.

Kramer, N., Cosca, M.A., and Hunziker, J.C., 2001, Heterogeneous ^{40}Ar distribution in naturally deformed muscovite: in situ UV-laser ablation evidence for microstructurally controlled intragrain diffusion: Earth and Planetary Science Letters 192, p. 377-388.

Lagos, M., Scherer, E.E., Tomaschek, F., Münker, C., Keiter, M., Berndt, J., Ballhaus, C., 2007. High precision Lu–Hf geochronology of Eocene eclogite-facies rocks from Syros, Cyclades, Greece: Chemical Geology 243, p. 16-35.

Lanari, P., Guillot, S., Schwartz, S., Vidal, O., Tricart, P., Riel, N., Beyssac, O., 2012: Diachronous evolution of the alpine continental subduction wedge: Evidence from P–T estimates in the Brianc¸ onnais Zone houillère (France – Western Alps): Journal of Geodynamics 56-57, p. 39-54.

Lanari, P., Vidal, O., De Andrade, V., Dubacq, B., Lewin, E., Grosch, E., Schwartz, S., 2014: XMapTools: a MATLAB©-based program for electron microprobe X-ray image processing and geothermobarometry. Computers and Geosciences. 62, 227-240.

Lee, J.K.W., 1995. Multipath diffusion in geochronology: Contributions to Mineralogy and Petrology 120, p.60-82.

McDougall, I., and Harrison, T.M., 1999, Geochronology and Thermochronology by the $^{40}Ar/^{39}Ar$ Method, 2nd ed.: Oxford University Press, New York, 288 p.

Mulch, A., Cosca, M., Handy, M., 2002. In-situ UV-laser 40Ar/39Ar geochronology of a micaceous mylonite: an example of defect-enhanced argon loss. Contributions to Mineralogy and Petrology 142 (6), 738–752.

Papanikolaou, D.J., 1987, Tectonic evolution of the Cycladic Blueschist Belt (Aegean Sea, Greece). H.C. Helgeson, Chemical Transport in Metasomatic Processes, p. 429-450.

Passchier, C.W., 2001, Flanking structures: Journal of Structural Geology 23, p. 951-962.

Philippon, M., Brun, J.P., and Gueydan, F., 2011, Tectonics of the Syros blueschists(Cyclades, Greece): From subduction to Aegean extension: Tectonics 30, TC4001,doi:10.1029/2010TC002810.

Ring, U., Glodny, T., Will, T., and Thomson, S., 2010, The Hellenic subduction system: High-pressure metamorphism, exhumation, normal faulting and large-scale extension: Annual Reviews of Earth and Planetary Sciences 38, p. 45-76.

Rogowitz, A., Grasemann, B., Huet, B., and Habler, G., 2014, Strain rate dependent calcite microfabric evolution – An experiment carried out by nature: Journal of Structural Geology 69, p- 1-17.

Rolland, Y., Cox, S.F., Corsini, M., 2009, Constraining deformation stages in brittle–ductile shear zones from combined field mapping and $^{40}Ar/^{39}Ar$ dating: The structural evolution of the Grimsel Pass area (Aar Massif, Swiss Alps): Journal of Structural Geology 31, p. 1377-1394.

Sanchez, G., Rolland, Y., Schneider, J., Corsini, M., Oliot, E., Goncalves, P., Verati, C., Lardeaux, J., Marquer, D., 2011, Dating low-temperature deformation by

40Ar/39Ar on white mica, insights from the Argentera-Mercantour Massif (SW Alps): Lithos 125, p. 521-536.

Schneider, S., Hammerschmidt, K., Rosenberg, C., 2013. Dating the longevity of ductile shear zones: Insight from 40Ar/39Ar in situ analyses. Earth and Planetary Science Letters, 369-370, 43–58.

Schumacher, J.C., Brady, J.B., Cheney, and J.T., Tonnsen, R.R., 2008, Glaucophane-bearing marbles on Syros, Greece: Journal of Petrology 49, p. 1667-1686.

Sigoyer, J., Chavagnac, V., Blichert-Toft, J., Villa, I.M., Luais, B., Guillot, S., Cosca, M., and Mascle, G., 2000, Dating the Indian continental subduction and collisional thickening in the northwest Himalaya: Multichronology of the Tso Morari eclogites: Geology 28, p. 487-490.

Soukis, K., and Stockli, D.F., 2013, Structural and thermochronometric evidence for multi-stage exhumation of southern Syros, Cycladic islands, Greece: Tectonophysics 595-596, p. 148-164.

Tomaschek, F., Baumann, A., Villa, I.M., Kennedy, A., and Ballhaus, C., 2000, Geochronological constraints on a Cretaceous metamorphic event from the Vari Unit (Syros, Cyclades, Greece): Beihefte zum European Journal of Mineralogy 12, 214.

Tomaschek, F., Kennedy, A.K., Villa, I.M., Lagos, M., and Ballhaus, C., 2003, Zirkons from Syros, Cyclades, Greece-recrystallization and mobilization of zircon during high-pressure metamorphism. Journal of Petrology 44, p.1977-2002.

Trotet, F., Jolivet, L., and Vidal, O., 2001a, Tectono-metamorphic evolution of Syros and Sifnos islands (Cyclades, Greece): Tectonophysics 338, p. 179-206.

Trotet, F., Vidal, O., and Jolivet, L., 2001b, Exhumation of Syros and Sifnos metamorphic rocks (Cyclades, Greece). New constraints on the P-T paths: European Journal of Mineralogy 13, p. 901-920.

Warren, C., Hanke, F., and Kelley, S., 2012, When can muscovite ^{40}Ar/^{39}Ar dating constrain the timing of metamorphic exhumation?: Chemical Geology 291, p. 79-86.

Wijbrans J.R., and McDougall, I., 1986, ^{40}Ar/^{39}Ar dating of white micas from an Alpine high-pressure metamorphic belt on Naxos (Greece): the resetting of the argon isotopic systems: Contributions to Mineralogy and Petrology, 93, p. 187-194.

Wortel, M.J.R., Goes, S.D.B., and Spakman, W., 1993, Structure and seismicity of the Aegean subduction zone: Terra Nova 2, p. 554-562.

Figure captions

Fig. 1. Outcrop photographs exhibiting two opposing shear directions. **A**, **B.** Asymmetric boudinaged dolomite layers in marble showing evidence of top-to-west shear.**C.** Sheared calcite sigma-clast indicating top-to-east sense of shear. **D.** a-type flanking structure indicating overall top-to-east sense of shear resulting in local antithetic shearing. HR and SZ indicate the location of the sampled host rock and shear zone, respectively.

Fig. 2. A-D Photomicrographs of calcite marble (crossed-polarizers). **A.** Host rock marble showing minor undulatory extinction and grain boundary migration. **B.** Transition from host rock to protomylonitic and unltramylonitic marble within the shear zone. **C.** Host rock marble showing preferred alignment of mica grains **D.** Shear zone showing locally brittle deformed mica surrounded by recrystallised calcite. **E.** BSE-image of prismatic white mica in host rock marble. Note that a lack of grey shade variation is an indication of no chemical zoning. **F.** BSE-image of brittlely deformed white mica within the shear zone marble.

Fig. 3. Mineral geochemistry results from the calcite marble on Syros. **A.** X_{Mg} vs. Si plot of phengite from within the host rock (HR, light grey) and the shear zone (SZ, dark grey) illustrating high Si and extremely low Fe content in mica. Shaded areas represent the range of compositions generated with Monte Carlo simulations. **B.** Ternary diagrams of white mica composition. Note that there is no compositional difference between host rock and shear zone mica (See Table S2 in the supplementary material for chemical analyses). End-member abbreviations: Ms: muscovite, Cel: celadonite, Prl: pyrophyllite and Pg: paragonite.

Fig. 4. A. $^{40}Ar/^{39}Ar$ age step-heated release spectra for phengite located within the host rock (HR, light grey) and shear zone (SZ, dark grey) on Syros. Note that both spectra yield concordant ages. Tg: total-gas age. Tp: preferred age (See Table S1 in

the supplementary material for analytical results). **B.** $^{38}Ar/^{39}Ar$ vs. $^{37}Ar/^{39}Ar$ graph illustrating a potential isochemical population for the shear zone mica analyses and a more heterogeneous chemical population for host rock mica. The individual steps are labelled, and correspond to the steps on the spectra (Table S1).

Fig. 5. Equilibrium assemblage diagram demonstrating the stability field of the observed high variance mineral assemblage (Ph + Cal + Qtz + Dol) of the calcite marble on Syros. Calculation was done in the CaKMASHC system with the PERPLEX 6.6.8 (Connolly, 1990) package using the Holland & Powell (1998) database. Solid solutions were considered for white mica (Coggon & Holland, 2002), carbonates (Holland &Powell, 1998) and H_2O-CO_2 fluid (Holland & Powell, 1998). Excluded phases are zoisite, sanidine and vesuvianite. Bulk rock composition was calculated using mineral fractions and EMP analyses (SiO_2: 4.47, Al_2O_3: 1.68, MgO: 0.40, CaO: 92.67, K_2O: 0.78 wt%). Pressure-temperature and fluid composition are likely to have varied during the metamorphic evolution of the studied rocks. The phase diagram was therefore calculated along variable H_2O-CO_2 fluid composition (x-axis) and a linear gradient (from 550 °C, 18 kbar to 300 °C, 4 kbar; y-axis) that approximates the P-T path of Syros (Trotet et al., 2001b; Schumacher et al., 2008). Mineral abbreviations: Qtz: quartz, Dol: dolomite, Clc: clinochlore, Phl: phlogopite, Ph: phengite, Tr: tremolite, Kfs: potassium feldspar, Di: diopside, Tlc: talc, Arg: aragonite and Cal: calcite.

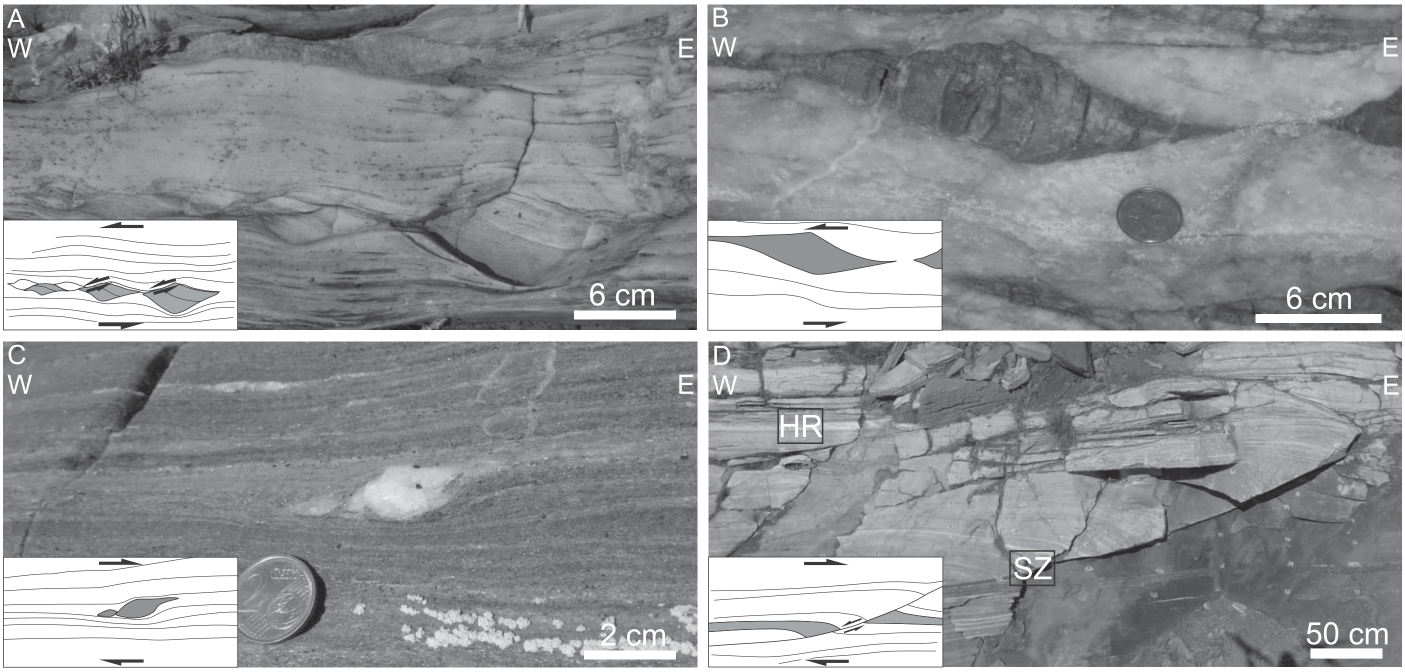

This is the accepted manuscript version of the final article:
Anna Rogowitz, Benjamin Huet, David Schneider, and Bernhard Grasemann (2015):
Influence of high strain rate deformation on 40Ar/39Ar mica ages from marble mylonites (Syros, Greece), Lithosphere, 7, 535-540
The final paper is accessible via http://dx.doi.org/10.1130/L455.1

Figure2

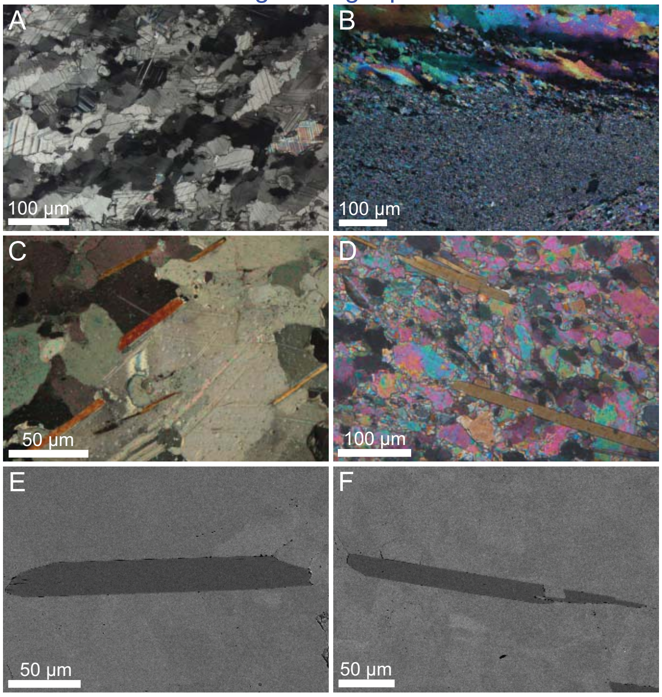

This is the accepted manuscript version of the final article:
Anna Rogowitz, Benjamin Huet, David Schneider, and Bernhard Grasemann (2015):
Influence of high strain rate deformation on 40Ar/39Ar mica ages from marble mylonites (Syros, Greece), Lithosphere, 7, 535-540
The final paper is accessible via http://dx.doi.org/10.1130/L455.1

Figure3
Click here to download Figure: Fig.3.pdf

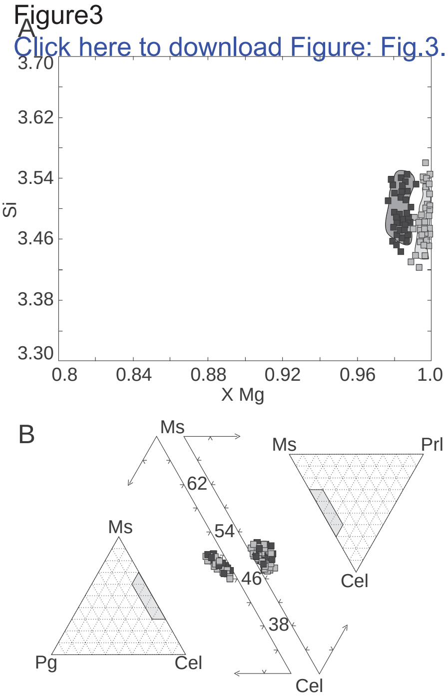

This is the accepted manuscript version of the final article:
Anna Rogowitz, Benjamin Huet, David Schneider, and Bernhard Grasemann (2015):
Influence of high strain rate deformation on 40Ar/39Ar mica ages from marble mylonites (Syros, Greece), Lithosphere, 7, 535-540
The final paper is accessible via http://dx.doi.org/10.1130/L455.1

Figure4

Click here to download Figure: Fig.4.pdf

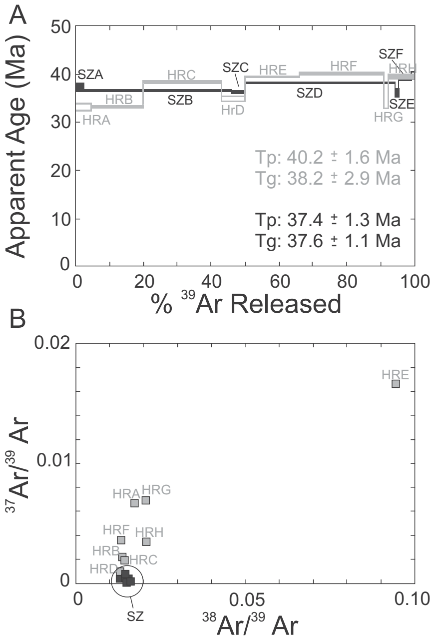

This is the accepted manuscript version of the final article:
Anna Rogowitz, Benjamin Huet, David Schneider, and Bernhard Grasemann (2015):
Influence of high strain rate deformation on 40Ar/39Ar mica ages from marble mylonites (Syros, Greece), Lithosphere, 7, 535-540
The final paper is accessible via http://dx.doi.org/10.1130/L455.1

Figure5

Click here to download Figure: Fig.5.pdf

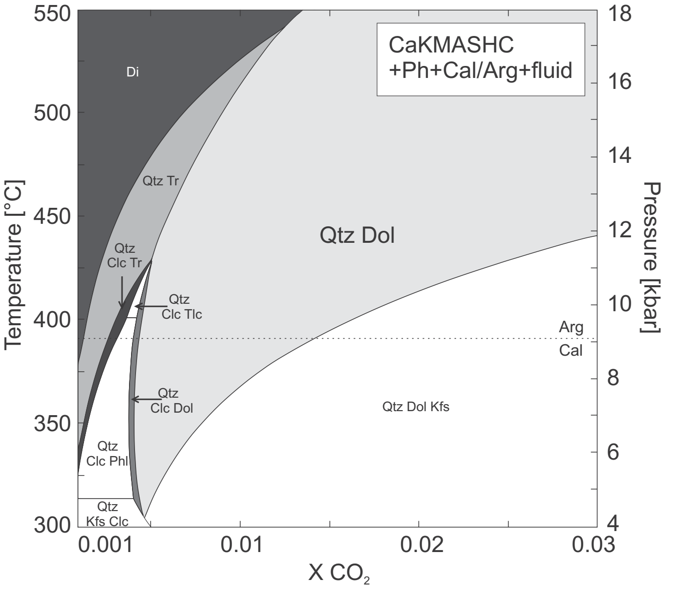

This is the accepted manuscript version of the final article:
Anna Rogowitz, Benjamin Huet, David Schneider, and Bernhard Grasemann (2015):
Influence of high strain rate deformation on 40Ar/39Ar mica ages from marble mylonites (Syros, Greece), Lithosphere, 7, 535-540
The final paper is accessible via http://dx.doi.org/10.1130/L455.1